Hydrated lithium intercalation into the Kitaev spin liquid candidate material α-$RuCl_3$

Yoshinori Imai,* Katsuya Konno, Yoshinao Hasegawa, Takuya Aoyama, and Kenya Ohgushi
Department of Physics, Tohoku University, 6-3 Aramaki-Aoba, Aoba-ku, Sendai, Miyagi 980-8578, Japan

(Received 23 April 2019; published 21 June 2019)

We study the transport and magnetic properties of hydrated and lithium-intercalated α-$RuCl_3$, $Li_xRuCl_3 \cdot yH_2O$, to investigate the effect on mobile-carrier doping into candidate materials for a realization of a Kitaev model. From thermogravimetric and one-dimensional electron map analyses, we find two crystal structures of this system, that is, monolayer hydrated $Li_xRuCl_3 \cdot yH_2O$ ($x \approx 0.56$, $y \approx 1.3$) and bilayer hydrated $Li_xRuCl_3 \cdot yH_2O$ ($x \approx 0.56$, $y \approx 3.9$). The temperature dependence of the electrical resistivity shows a temperature hysteresis at 200–270 K, which is considered to relate to the formation of a charge order. The antiferromagnetic order at 7–13 K in pristine α-$RuCl_3$ is successfully suppressed down to 2 K in bilayer hydrated $Li_xRuCl_3 \cdot yH_2O$, which is sensitive to not only the electronic state of Ru but also the interlayer distance between Ru-Cl planes.

DOI: 10.1103/PhysRevB.99.245141

I. INTRODUCTION

Triggered by a proposal of a new quantum model called the Kitaev model [1], a tremendous number of studies have been performed on a quantum spin liquid, especially a Kitaev quantum spin liquid [2–5]. The Kitaev model is a very simple model where $S = 1/2$ spins are placed on a honeycomb lattice and are coupled with a nearest-neighbor bond-dependent interaction. The most remarkable feature of the Kitaev model is that this is an exactly solvable model, which shows that the ground state is the Kitaev quantum spin liquid and that Majorana fermions emerge as excitations [6–8]. Since bond-dependent interactions naturally exist in materials with strong spin-orbit couplings [9,10], some compounds with unfilled $4d/5d$ orbitals have been attracting intensive attention [4]. Especially, α-$RuCl_3$ is the most likely candidate material for the Kitaev quantum spin liquid since $J_{\rm eff} = 1/2$ spins are coupled with each other through the Kitaev-type ferromagnetic interactions [11].

The space group of $RuCl_3$ is $C2/m$ [12], and honeycomb lattices of octahedrally coordinated Ru^{3+} ions are stacked via a van der Waals interaction. The Ru^{3+} ions have a low-spin configuration of $(t_{2g})^5$, bearing effective $J_{\rm eff} = 1/2$ spins. Contrary to expectations from the Kitaev model, $RuCl_3$ shows an antiferromagnetic (AF) transition around an AF transition temperature, $T_N = 7$–13 K, which is considered to be due to non-Kitaev interactions, such as direct exchange interactions and next-nearest-neighbor superexchange interactions. Recent investigations assigned the phase with $T_N \sim 7$ K to an *ABC* stacking order and that with $T_N \sim 13$ K to an *AB* stacking fault [12,13]. However, upon the application of in-plane magnetic fields, an antiferromagnetic order is fully suppressed down to the lowest temperature, and the half-integer quantization is observed in the thermal Hall conductance measurement, which provides direct evidence for capturing Majorana fermions [14].

The study on the substitution effect for $RuCl_3$ is intriguing to reveal the role of impurities for realization of the Kitaev model, and earlier studies on $(Ru_{1-x}Ir_x)Cl_3$ clarified that the spin-liquid-like state appears in the wide range of an electronic phase diagram [15,16]. Introduction of not localized impurities but, rather, mobile charge carriers into $RuCl_3$ is a more challenging issue [15–19] because some theoretical studies predict the emergence of novel superconductivity in the carrier-doped Kitaev material [20–27]. In the electron-doped material $K_{0.5}RuCl_3$ [a formal valence is $Ru^{2.5+}$ with the $(4d)^{5.5}$ electron configuration], which is prepared by K coating on a $RuCl_3$ single crystal cleaved in a vacuum chamber, a charge order of $(4d)^5$ and $(4d)^6$ states is proposed at low temperatures [17]. The Li-intercalated material Li_xRuCl_3 prepared by using $LiBH_4$ reveals that the antiferromagnetic order is suppressed below 2 K and that the electrical resistivity still remains an insulating behavior [18,19]. In the study, the Li content x is as low as $x = 0.2$, which is smaller than the honeycomb-lattice percolation threshold, $x_p = 0.303$. Therefore, studies over a wide carrier concentration range are highly expected for understanding the doping effect on Kitaev materials.

Here, we report on the successful preparation of hydrated and Li-intercalated $RuCl_3$, in which electron carriers are doped into $RuCl_3$ by using a soft-chemical method, and an investigation of their electronic properties. In $Li_xRuCl_3 \cdot yH_2O$, there are two kinds of crystal structures, i.e., monolayer hydrate (MLH) and bilayer hydrate (BLH). The AF state is completely suppressed down to 2 K in BLH-$Li_xRuCl_3 \cdot yH_2O$. It turns out that T_N depends on an electronic state of Ru as well as the distance between Ru-Cl layers.

II. EXPERIMENT

We prepare eight samples of α-$RuCl_3$and hydrated and Li-intercalated $RuCl_3$, whose detailed specifications are summarized in Table I. Commercially available α-$RuCl_3$ polycrystalline powders (3N, Mitsuwa Chemicals) were used as a pristine sample in this study, which is represented as sample

*imai@tohoku.ac.jp

TABLE I. Specification of samples used in this study. "MLH" and "BLH" in a composition indicate that the sample is a monolayer hydrate and a bilayer hydrate, respectively. Details for method 1 and method 2 in the postprocess are described in the text. The lattice parameters (a, b, c, β) are deduced under the assumption of monoclinic space group $C2/m$. The parameter c^* represents the interlayer distance of the Ru-Cl plane. In the column for antiferromagnetic transition temperature T_N, <2 K indicates that an antiferromagnetic transition does not appear above 2 K in the magnetic susceptibility measurements.

	Composition	Form	Solvent	Postprocess	c^* (Å)	a (Å)	b (Å)	c (Å)	β (deg)	T_N (K)
Sample A	$RuCl_3$	polycrystal	-	-	5.72	5.98	10.36	6.04	108.9	13.2 K
Sample B	BLH-$Li_xRuCl_3 \cdot yH_2O$	polycrystal	ethanol		11.12	6.04	10.43	11.16	90.1	<2 K
Sample C	BLH-$Li_xRuCl_3 \cdot yH_2O$	polycrystal	2-propanol		10.95	6.04	10.48	11.02	90.1	<2K
Sample D	MLH-$Li_xRuCl_3 \cdot yH_2O$	polycrystal	ethanol	method 1	8.17	6.03	10.35	8.25	98.3	3.6 K
Sample E	BLH-$Li_xRuCl_3 \cdot yH_2O$	polycrystal	ethanol	method 2	11.22	6.03	10.42	11.27	90.0	<2K
Sample F	$RuCl_3$	single crystal			5.73					7.5 K, 13.2 K
Sample G	MLH-$Li_xRuCl_3 \cdot yH_2O$	single crystal	ethanol	method 1	8.23					3.6 K
Sample H	BLH-$Li_xRuCl_3 \cdot yH_2O$	single crystal	ethanol	method 2	10.98					<2K

A in Table I. Hydrated Li-intercalated samples are prepared as follows. $RuCl_3$ powders of 0.3 g were soaked in a 1.5 mol/L LiI solution of ethanol (2-propanol), which contains a few percent of water, at their boiling point for 2 h. This reaction can be described by the following chemical reaction formula: $RuCl_3 + xLiI + yH_2O \rightarrow Li_xRuCl_3 \cdot yH_2O + \frac{x}{2}I_2$. Then, the samples are washed in the same liquid as a solvent and dried at room temperature, which is sample B (sample C). To clarify whether H_2O is actually intercalated into samples, we tried two kinds of postprocess for sample B. At first, powders of sample B are kept with silica gel in a sealed vessel for 1 day; this process is called method 1. The obtained sample is named sample D in Table I. Next, we store sample D with wet cotton in a sealed vessel for 1 day; this process is called method 2. The product is named sample E in Table I. $RuCl_3$ single crystals (sample F) were prepared by the chemical vapor transport method as described elsewhere [28,29]. Some pieces of $RuCl_3$ single crystals (typical size: $2 \times 2 \times 0.1$ mm^3) were soaked in a 1.5 mol/L LiI solution of ethanol at room temperature for 24 h and then washed by ethanol before drying at room temperature. After that, intercalated crystals were kept in a sealed vessel with silica gel or wet cotton for 1 day, which are samples G and H in Table I, respectively.

All the products were characterized by powder x-ray diffraction (XRD) using Cu $K\alpha$ radiation at room temperature. The chemical composition was determined by the inductively coupled plasma (ICP) atomic emission spectroscopy and thermogravimetry analysis. The electrical resistivity ρ was measured by the four-terminal method over the temperature range of 77 to 300 K. The current direction is along the ab plane. Magnetic susceptibility measurements were performed using a superconducting quantum interference device magnetometer.

III. RESULTS

Figure 1(a) shows XRD patterns for polycrystalline samples A–E. All peaks can be indexed on the basis of a monoclinic space group (No. 12, $C2/m$) [12], and calculated lattice parameters are summarized in Table I. The peak positions of $00l$ peaks for intercalated samples shift toward smaller 2θ values than those for a pristine sample (sample A), indicating successful intercalation. It is highly unlikely that this considerable increase in the interlayer distance c^* between Ru-Cl layers results from the intercalation of only Li ions because in other Li-intercalated materials such as Li_xTaS_2 and Li_xNbS_2, the increase of interlayer distance is known to be as small as 1 Å [30,31]. Thus, it is quite reasonable that some kinds of molecules are cointercalated with Li ions. Here, it should be noted that the peak positions of samples B and C, which are respectively synthesized in ethanol and 2-propanol as solvents, are almost the same, indicating that the intercalated molecule is the same one in samples B and C. The most likely candidate of the intercalated molecule in both samples B and C is H_2O, which is included in both ethanol and 2-propanol. To clarify whether the H_2O molecule is actually cointercalated with Li ions in samples B and C, we tried two kinds of postprocess described above for sample B. In XRD patterns of sample D, which had been kept in silica gel through the postprocess of method 1, the positions of $00l$ peaks shift towards larger 2θ values; the c^* value decreases by $\sim$3 Å from c^* of sample B. Interestingly, when sample D is kept under high humidity for 1 day through the postprocess of method 2, the positions of $00l$ shift towards smaller 2θ values again, and the resultant XRD pattern of sample E is the same as that of sample B. This shows that the intercalated molecules exist not only in the solvent but also in air, which indicates that the cointercalated molecule is H_2O. We can then conclude that there are two types of structure forms with the chemical formula $Li_xRuCl_3 \cdot yH_2O$ with the same x value and distinct y values. The crystal structure with a larger (smaller) y value has a longer (shorter) interlayer distance. Comparing the lattice constants between pristine and intercalated samples, interesting changes are observed in the parameter of β. The angle of β gets close to a value of 90° with increasing c^*, which indicates that the monoclinic distortion is relaxed by the intercalation of Li and H_2O. Therefore, it is expected that the ideal honeycomb lattice with a smaller distortion is realized in the intercalated samples compared to pristine $RuCl_3$.

In order to determine the chemical compositions x and y for two structural forms, we first performed the ICP analysis for sample B with a longer interlayer distance c^*. This reveals that the ratio of Li and Ru is $0.56 \pm 0.02 : 1$ ($x = 0.56$). Since it is likely that there is no difference in Li concentration x between two crystal forms, we can postulate $x = 0.56$ for sample D with a smaller c^* value. We then perform thermogravimetric

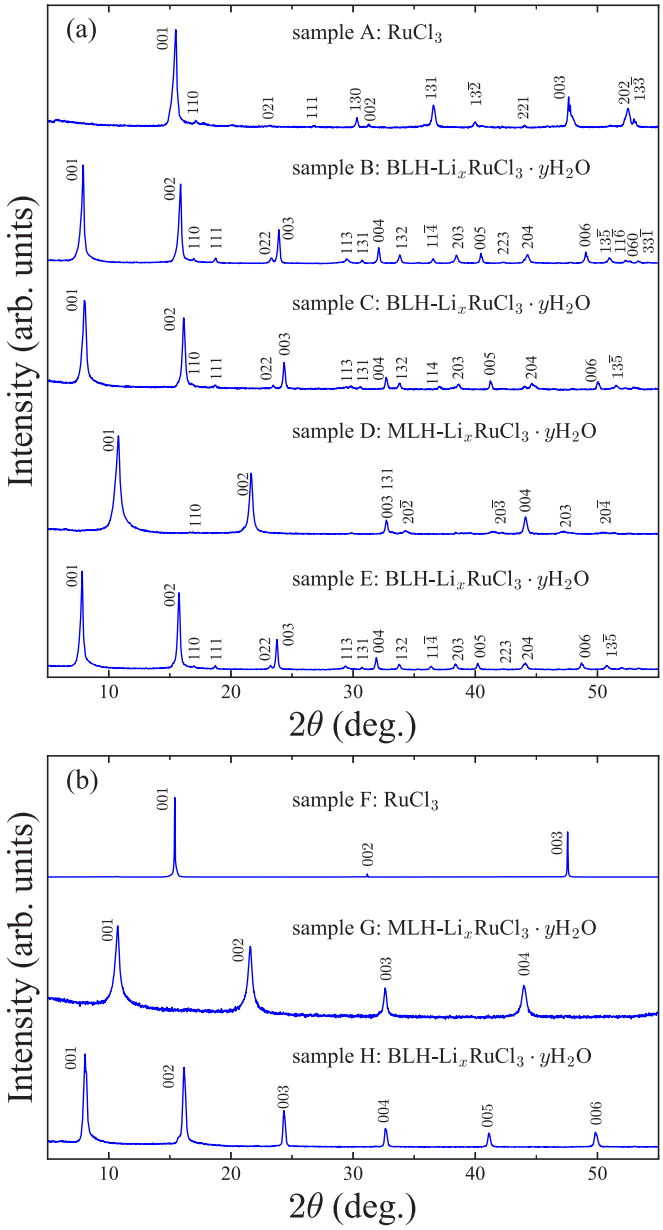

FIG. 1. X-ray diffraction patterns for (a) polycrystals of samples A–E and (b) single crystals of samples F–H. The vertical axis is in a logarithmic scale. The Miller indexes on the basis of the monoclinic $C2/m$ are also shown.

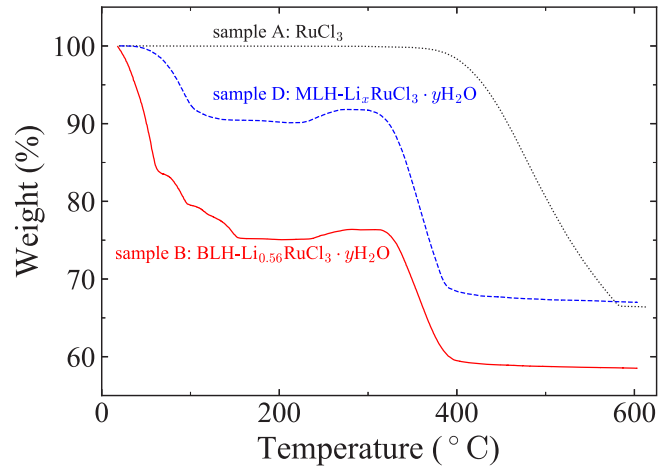

FIG. 2. Thermogravimetric analysis for samples A, B, and D in the heating process up to 600 °C at 1°C/min. The temperature dependence of weight loss is shown.

analysis for samples A, B, and D on heating at 1°C/min in air, as shown in Fig. 2. The weight of samples B and D decreases from room temperature to ∼220 °C, while sample A remains unchanged up to ∼300 °C. The observed decrease in the weight of samples B and D likely corresponds to a reaction of $Li_xRuCl_3 \cdot yH_2O \rightarrow Li_xRuCl_3$, and one can estimate the H_2O content, $y = 3.9 \pm 0.1$ for sample B and $y = 1.3 \pm 0.1$ for sample D. The weight loss at temperatures higher than ∼300 °C observed in samples A, B, and D results from the decomposition and oxidization of $RuCl_3$ into Ru oxides and Cl_2. We consider that the intercalated single crystals (sample G and H) take the same compositions. Here, it should be noted that the pristine $RuCl_3$ itself is stable in air. The recent Raman spectroscopy measurements for exfoliated $RuCl_3$ single crystals revealed that the Raman spectra for monolayer single crystals of $RuCl_3$ were reproducible after months of exposure to air and that the H_2O molecule was not intercalated into $RuCl_3$ [32]. In addition, we confirm that soaking $RuCl_3$ in ethanol does not change the lattice constant. This is in sharp contrast to the hydrated and Li-intercalated $Li_xRuCl_3 \cdot yH_2O$, which changes its water content y in response to changes in humidity even at room temperature. The moisture-sensitive behavior, which is similar to the cobalt oxyhydrate superconductor $Na_xCoO_2 \cdot yH_2O$ [33,34], is observed only in $Li_xRuCl_3 \cdot yH_2O$.

To obtain information on the location of Li and H_2O, we perform a detailed analysis of XRD patterns for single-crystalline samples [Fig. 1(b)], where only $00l$ peaks are observed. We obtain one-dimensional (1D) electron density (ED) map profiles projected along the stacking axis (defined as the c^* axis). The methodology for the calculation of a 1D ED map in this study is described in detail elsewhere [18,35]. When one considers only $00l$ reflections, the distribution of the scattering density projected on the c^* axis ρ_z is calculated by the Fourier summation

$$\rho_z = \frac{1}{c^*} \sum_l F_{00l} \exp(-i2\pi lz), \tag{1}$$

in which F_{00l} is the structure factor for $00l$ peaks. To calculate ρ_z, the phase of F_{00l} is necessary, while the absolute value of F_{00l} can be estimated from the integrated intensity of the $00l$ peak I_{00l} in the XRD patterns. The phases are constrained to one of two values, that is, zero or π, because of the centrosymmetric projection in this study, and these values are determined based on the phases of structural factors for $RuCl_3$ [12,36]. This estimation is reasonable under the assumption that the contribution for the scattering from the intercalated ions or molecules is smaller than that from the $RuCl_3$ component. After the estimation of the structural model from the 1D ED map, the sign of F_{00l} is checked by recalculating the structural factors from the scattering of all components, including intercalated atoms and molecules [36].

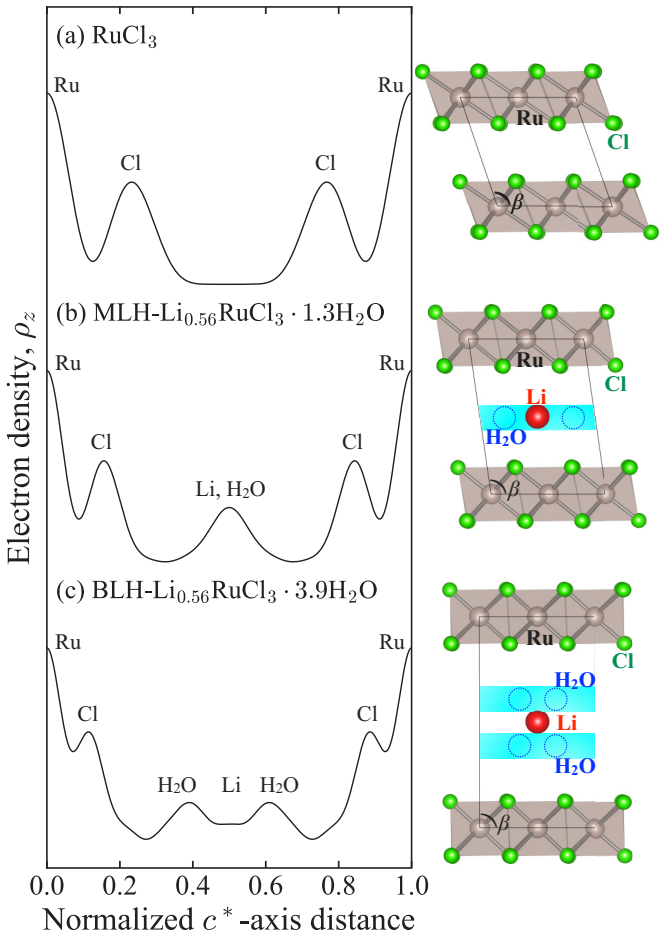

FIG. 3. One-dimensional electron density map ρ_z and the structural model of the *ac* plane for single crystals of (a) $RuCl_3$ (sample F) and (b) MLH- and (c) BLH-$Li_xRuCl_3 \cdot yH_2O$ (samples G and H).

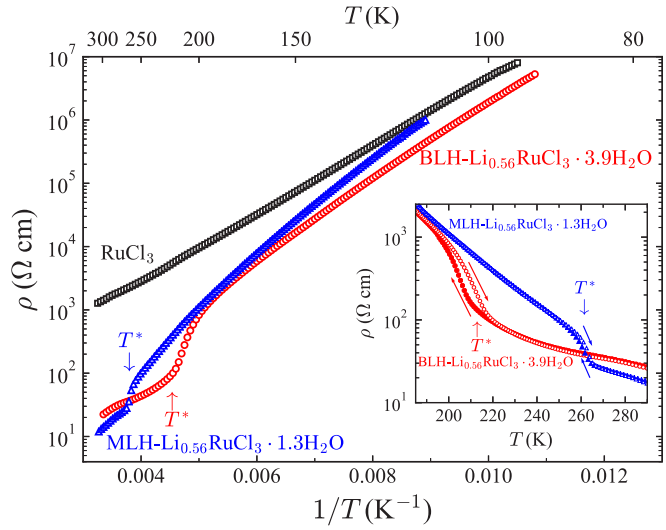

FIG. 4. Arrhenius plot of the in-plane resistivity ρ for single crystals of $RuCl_3$ and MLH- and BLH-$Li_xRuCl_3 \cdot yH_2O$ (samples F–H). The inset shows the resistivity in cooling and warming cycles, which are represented by solid and open symbols, respectively, in the vicinity of the phase transition temperature T^*.

Figure 3 shows the 1D ED map of $RuCl_3$ (sample F) and $Li_xRuCl_3 \cdot yH_2O$ with $x \approx 0.56$, $y \approx 1.3$ (sample G) and $x \approx 0.56$, $y \approx 3.9$ (sample H). In spite of the constraint on values of phases for F_{00l}, the 1D ED map profile of $RuCl_3$ [Fig. 3(a)] is consistent with the atomic position of $RuCl_3$, which indicates that the calculation method is reliable. The 1D ED map profile for $Li_xRuCl_3 \cdot yH_2O$ with $x \approx 0.56$, $y \approx 1.3$ (sample G) shows that the electron density due to guest atoms and molecules forms a single peak around the center of the gallery. On the other hand, for $Li_xRuCl_3 \cdot yH_2O$ with $x \approx 0.56$, $y \approx 3.9$ (sample H), the contributions of the intercalated atoms and molecules are observed as a small hump in the center part and two broad peaks placed 1.2 Å below and above the center of the gallery. Here, we recall that there are many layered hydrates with the general formula $A_x(MX_2) \cdot yH_2O$ (A = alkali metal, M = transition metals, and X = O, S). These layered hydrates generally have two kinds of crystal structures, i.e., MLH and BLH, where a single cation and H_2O layer or a sequence of H_2O-cation-H_2O layers separates the electron-doped two-dimensional MX_2 layers by distances of ∼7 or ∼10 Å, respectively. $Na_xCoO_2 \cdot yH_2O$ with a triangular Co sublattice is a typical material in the above series: BLH-$Na_xCoO_2 \cdot yH_2O$ ($x \approx 0.35$, $y \approx 1.3$) shows superconductivity with a superconducting temperature of ∼5 K [33], while superconductivity is not observed in MHL-$Na_xCoO_2 \cdot yH_2O$ ($x \approx 0.35$, $y \approx 0.7$) [34]. We note that 1D ED maps for samples G and H in Fig. 3 are similar to the electron density for MLH- and BLH-$Na_xCoO_2 \cdot yH_2O$. In addition, the variations in c^* for samples F–H shown in Table I are similar to those in the anhydrous Na_xCoO_2 and MLH- and BLH-$Na_xCoO_2 \cdot yH_2O$, whose interlayer distances are 5.5, 6.9, and 9.8 Å, respectively [33,34]. Therefore, we conclude that sample G is MLH-$Li_{0.56}RuCl_3 \cdot 1.3H_2O$, where Ru-Cl layers are separated by a single layer of Li and $H_2O$and that sample H is BLH-$Li_{0.56}RuCl_3 \cdot 3.9H_2O$, where Ru-Cl layers are separated by layers of H_2O-Li-H_2O. Schematic pictures of crystal structures for these materials are shown in Fig. 3.

Figure 4 shows the temperature dependence of resistivity ρ for single crystals of $RuCl_3$ and MLH- and BLH-$Li_xRuCl_3 \cdot yH_2O$ (samples F–H). A pristine $RuCl_3$ single crystal, which is a strongly spin orbital coupled Mott insulator, shows a thermally activated type of temperature dependence, and the activation energy is $E_g \sim 0.093$ eV. This value is lower than that reported in polycrystalline $RuCl_3$ [18]. The resistivity for MLH- and BLH-$Li_xRuCl_3 \cdot yH_2O$ at room temperature is ∼2 orders of magnitude smaller than that of pristine $RuCl_3$. The intercalation of lithium ions makes the formal valence of Ru ions smaller than +3, so that the electron carriers are introduced into the material. These electron carriers are the origin for the decrease in ρ around room temperature. The activation energy around room temperature is $E_g \sim 0.12$ eV for MHL-$Li_xRuCl_3 \cdot yH_2O$ and $E_g \sim 0.092$ eV for BLH-$Li_xRuCl_3 \cdot yH_2O$, which are comparable with or slightly larger than that of pristine $RuCl_3$. On cooling intercalated materials, the electrical resistivity shows an anomalous hysteresis at $T^* =$ 260–270 K for MHL-$Li_xRuCl_3 \cdot yH_2O$ and $T^* =$ 200–220 K for BLH-$Li_xRuCl_3 \cdot yH_2O$, indicating the presence of the first-order transitions. On further cooling below T^*, the resistivity

rapidly increases, and the activation energy increases up to ~0.13–0.16 eV, which is larger than E_g of $RuCl_3$.

Figure 5 shows the temperature dependence of magnetic susceptibility χ for single crystals of $RuCl_3$and MLH- and BLH-$Li_xRuCl_3 \cdot yH_2O$ (samples F–H) under a magnetic field of $\mu_0 H = 1$ T parallel to the ab plane and the c axis. As reported previously [37], in $RuCl_3$ single crystals, χ for $H//ab$ is much larger than that for $H//c$, which leads to the so-called Γ term of the spin-orbital coupling origin [2]. One can also find two magnetic transitions at $T_{N1} \sim 7.5$ K and $T_{N2} \sim 13.2$ K in the in-plane measurement. Recent investigations revealed that T_{N1} is characteristics of an ABC stacking ordered system, while T_{N2} is induced by the AB stacking faults [12,13]. For χ of $RuCl_3$ under $H//ab$, we perform a Curie-Weiss fit with a fitting function of $\chi = C/(T - \theta_{CW})$, with $C = N_A \mu_{eff}^2 / 3k_B$, where θ_{CW}, C, μ_{eff}, N_A, and k_B are the Weiss temperature, the Weiss constant, the effective magnetic moment, Avogadro's constant, and Boltzmann's constant, respectively. They are estimated to be $\theta_{CW} = 25$ K and $\mu_{eff} = 2.3\,\mu_B$/Ru, which are consistent with a previous report [37]. The intercalation of Li ions and H_2O molecules results in a drastic change in magnetic properties. The anisotropy of χ in $RuCl_3$ is greatly reduced by the intercalation. The magnitude relationship of χ is reversed, and χ for $H//c$ is slightly larger than χ for $H//c$. In MLH-$Li_xRuCl_3 \cdot yH_2O$, magnetic susceptibility shows a broad peak around $T_N \sim 3.6$ K, which is considered to be an AF transition. Surprisingly, an AF transition is fully suppressed at least down to 2 K in BLH-$Li_xRuCl_3 \cdot yH_2O$. From a Curie-Weiss fit for intercalated samples with a function of $\chi = (1-x)C/(T - \theta_{CW})$, the θ_{CW} and μ_{eff} values are $\theta_{CW} = 16$ K and $\mu_{eff} = 1.4\,\mu_B/Ru^{3+}$ for MLH-$Li_xRuCl_3 \cdot yH_2O$ and $\theta_{CW} = -15$ K and $\mu_{eff} = 1.6\,\mu_B/Ru^{3+}$ for BLH-$Li_xRuCl_3 \cdot yH_2O$, respectively, which indicates that the ferromagnetic interaction in $RuCl_3$ changes to a weak AF interaction owing to the intercalation.

IV. DISCUSSION

We now discuss electronic states realized in the Li- and H_2O-intercalated $RuCl_3$. The formal valence of Ru in MLH- and BLH-$Li_xRuCl_3 \cdot yH_2O$ ($x \approx 0.56$) is +2.44, so that there are roughly equal numbers of Ru^{3+} ions with the $(4d)^5$ electron configuration ($J_{eff} = 1/2$) and Ru^{2+} ions with the $(4d)^6$ electron configuration ($J_{eff} = 0$). In terms of the band picture, this corresponds to the quarter-filled $J_{eff} = 1/2$ bands, which is in stark contrast to the half-filled $J_{eff} = 1/2$ bands in $RuCl_3$. The doped electron carriers are expected to conduct smoothly in the system; however, this is not the case. The reasons why MLH- and BLH-$Li_xRuCl_3 \cdot yH_2O$ do not show a metallic behavior is likely related to the first-order transition at T^*. Taking into account that the numbers of populated Ru^{2+} and Ru^{3+} ions are almost equal on the bipartite honeycomb lattice, we consider that a charge order with the alternate arrangement of Ru^{2+} and Ru^{3+} ions occurs below T^*. The rapid increase of ρ below T^* is consistent with the formation of a charge order. If there are relevant fluctuations far above T^*, the nonmetallic behavior of intercalated samples at room temperature is also well accounted for. We note that a similar scenario is also proposed for K-coated $RuCl_3$, where photoemission spectra exhibit a gaplike feature at low temperatures [17]. In the

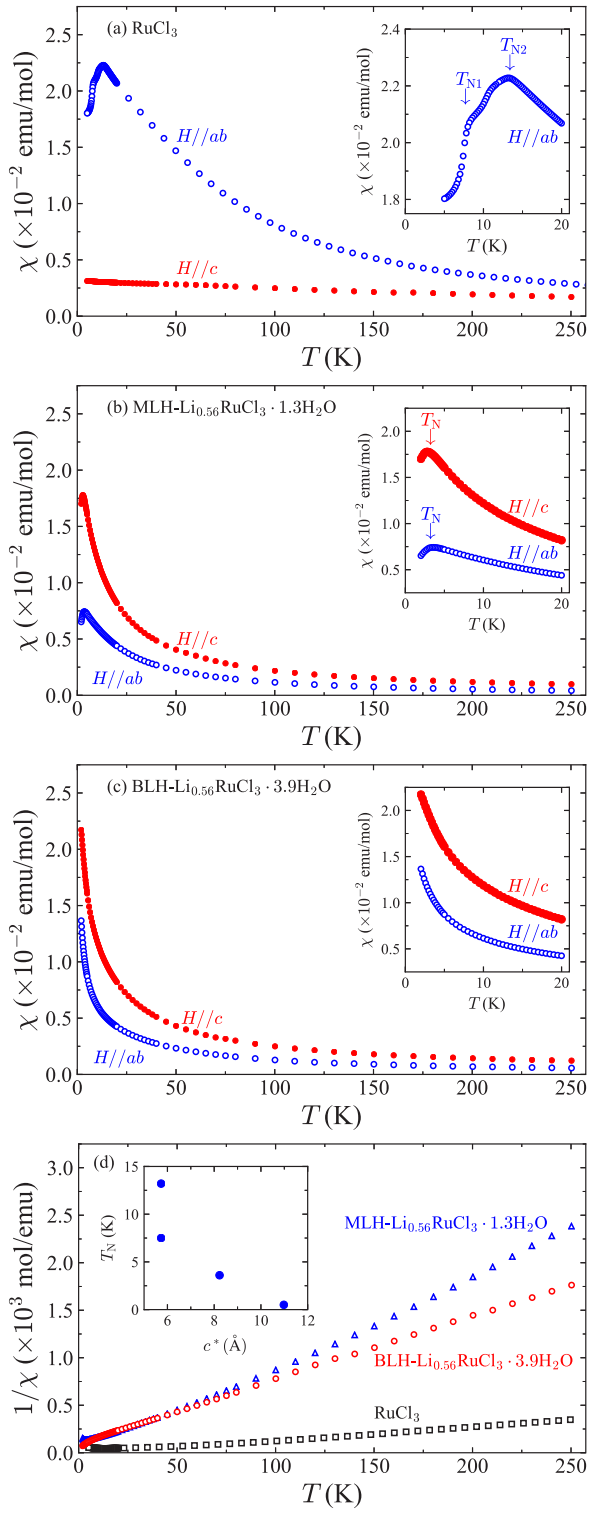

FIG. 5. Temperature dependences of magnetic susceptibility χ of single crystals of (a) $RuCl_3$ and (b) MLH- and (c) BLH-$Li_xRuCl_3 \cdot yH_2O$ at a magnetic field of $\mu_0 H = 1$ T parallel to the ab plane (open symbols) and the c axis (solid symbols). Insets are enlarged plots at low temperatures. (d) Curie-Weiss plot of χ under the magnetic fields parallel to the ab plane. The inset of (d) is the dependence of an antiferromagnetic transition temperature $T_N$on the interlayer distance c^*.

charge-ordered state, one set of Ru^{2+} and Ru^{3+} ions forms a triangular lattice, and the inversion symmetry is broken. Comparing T^* for MLH- and BLH-$Li_xRuCl_3 \cdot yH_2O$, the former is ~50 K higher than the latter. That is, the temperature where a charge order occurs is very different between MLH- and BLH-$Li_xRuCl_3 \cdot yH_2O$ in spite of the fact that these two samples have the same electron configuration. In the BLH system, Li ions are sandwiched between neutral H_2O layers, which results in the shielding of the Coulomb potential of Li ions. This may relate to the lower T^* in BLH-$Li_xRuCl_3 \cdot yH_2O$ than that in MLH-$Li_xRuCl_3 \cdot yH_2O$.

We next discuss the mechanism of the suppressed AF order in the intercalated $RuCl_3$. Because Ru^{2+} ions with $(4d)^6$ electron configurations are nonmagnetic and the doping level exceeds the percolation limit of a honeycomb lattice of 0.303, it is quite reasonable to expect the suppression of the AF order. More importantly, in the charge-ordered state, magnetic interactions across the nearest-neighbor Ru sites do not work since one of two adjacent Ru sites is occupied by a nonmagnetic Ru^{2+} ion. As a consequence, neither the Kitaev-type ferromagnetic interaction nor the so-called Γ term as a source of magnetic anisotropy works effectively, leading to isotropic spins. Instead, the next-nearest-neighbor interactions are expected to be dominant in the charge-ordered state. Therefore, the AF transition at low temperatures in MLH-$Li_xRuCl_3 \cdot yH_2O$ originates from exchange interactions on a Ru^{3+} triangular lattice. One plausible candidate of the AF structure in MLH-$Li_xRuCl_3 \cdot yH_2O$ is the 120° structure, which hosts the left-handed and right-handed chiralities. It should be noted that T_N for BLH-$Li_xRuCl_3 \cdot yH_2O$ is lower than that for MLH-$Li_xRuCl_3 \cdot yH_2O$, while the Li contents are the same in these two samples. This indicates that T_N depends on not only electronic states among honeycomb layers of Ru ions but also interlayer distances. As shown in the inset of Fig. 5(d), the longer the interlayer distance is, the lower the magnetic transition temperature is; this suggests that the interaction between Ru-Cl layers is the origin of the AF transition in MLH-$Li_xRuCl_3 \cdot yH_2O$ and well explains the absence of the magnetic order in BLH-$Li_xRuCl_3 \cdot yH_2O$. To realize the electron-doped Kitaev spin liquid, it is important to control the Li content precisely and clarify whether the Kitaev-like correlations remain or not in such a system.

V. SUMMARY

In summary, we successfully prepared hydrated and Li-intercalated α-$RuCl_3$, $Li_xRuCl_3 \cdot yH_2O$, by using a soft-chemical technique. We found two kinds of crystal structures; one is MLH-$Li_xRuCl_3 \cdot yH_2O$, and the other is BLH-$Li_xRuCl_3 \cdot yH_2O$. The interlayer distance between Ru-Cl layers for MLH- and BLH-$Li_xRuCl_3 \cdot H_2O$ is 1.4–1.9 times larger than that for pristine $RuCl_3$. MLH- and BLH-$Li_xRuCl_3 \cdot yH_2O$ do not show metallic behavior in the resistivity curves, while roughly half of the Ru sites change from Ru^{3+} to Ru^{2+}. We consider that this is due to the formation of a charge order at T^* where temperature hysteresis in the resistivity curves and a rapid increase of the resistivity are observed. The magnetic susceptibility measurements reveal that MLH-$Li_xRuCl_3 \cdot yH_2O$ shows an antiferromagnetic transition at $T_N = 3.61$ K and that an antiferromagnetic order is suppressed at least down to 2 K in BLH-$Li_xRuCl_3 \cdot yH_2O$, which suggests that the antiferromagnetic transition is sensitive to the electronic state of Ru and the interlayer distance.

ACKNOWLEDGMENTS

We would like to thank F. Sakamoto at Tohoku University for his help with the ICP analysis and Y. Motome at the University of Tokyo and J. Nasu at Yokohama National University for fruitful discussions. This work was supported by JSPS KAKENHI Grants No. 16K17732, No. 17H05474, No. 18H01159, No. 18H04302, No. 18K03531, and No. 19H04685.

[1] A. Kitaev, Ann. Phys. (NY) **321**, 2 (2006).
[2] S. M. Winter, A. A. Tsirlin, M. Daghofer, J. van den Brink, Y. Singh, P. Gegenwart, and R. Valentí, J. Phys.: Condens. Matter **29**, 493002 (2017).
[3] M. Hermanns, I. Kimchi, and J. Knolle, Annu. Rev. Condens. Matter Phys. **9**, 17 (2018).
[4] H. Takagi, T. Takayama, G. Jackeli, G. Khaliullin, and S. E. Nagler, Nat. Rev. Phys. **1**, 264 (2019).
[5] J. Knolle and R. Moessner, Annu. Rev. Condens. Matter Phys. **10**, 451 (2019).
[6] J. Knolle, D. L. Kovrizhin, J. T. Chalker, and R. Moessner, Phys. Rev. Lett. **112**, 207203 (2014).
[7] J. Knolle, G.-W. Chern, D. L. Kovrizhin, R. Moessner, and N. B. Perkins, Phys. Rev. Lett. **113**, 187201 (2014).
[8] J. Nasu, M. Udagawa, and Y. Motome, Phys. Rev. B **92**, 115122 (2015).
[9] G. Khaliullin, Prog. Theor. Phys. Suppl. **160**, 155 (2005).
[10] G. Jackeli and G. Khaliullin, Phys. Rev. Lett. **102**, 017205 (2009).
[11] K. W. Plumb, J. P. Clancy, L. J. Sandilands, V. V. Shankar, Y. F. Hu, K. S. Burch, H.-Y. Kee, and Y.-J. Kim, Phys. Rev. B **90**, 041112(R) (2014).
[12] R. D. Johnson, S. C. Williams, A. A. Haghighirad, J. Singleton, V. Zapf, P. Manuel, I. I. Mazin, Y. Li, H. O. Jeschke, R. Valentí, and R. Coldea, Phys. Rev. B **92**, 235119 (2015).
[13] H. B. Cao, A. Banerjee, J.-Q. Yan, C. A. Bridges, M. D. Lumsden, D. G. Mandrus, D. A. Tennant, B. C. Chakoumakos, and S. E. Nagler, Phys. Rev. B **93**, 134423 (2016).
[14] Y. Kasahara, T. Ohnishi, Y. Mizukami, O. Tanaka, S. Ma, K. Sugii, N. Kurita, H. Tanaka, J. Nasu, Y. Motome, T. Shibauchi, and Y. Matsuda, Nature (London) **559**, 227 (2018).
[15] P. Lampen-Kelley, A. Banerjee, A. A. Aczel, H. B. Cao, M. B. Stone, C. A. Bridges, J.-Q. Yan, S. E. Nagler, and D. Mandrus, Phys. Rev. Lett. **119**, 237203 (2017).
[16] S.-H. Do, W.-J. Lee, S. Lee, Y. S. Choi, K.-J. Lee, D. I. Gorbunov, J. Wosnitza, B. J. Suh, and K.-Y. Choi, Phys. Rev. B **98**, 014407 (2018).

[17] A. Koitzsch, C. Habenicht, E. Müller, M. Knupfer, B. Büchner, S. Kretschmer, M. Richter, J. van den Brink, F. Börrnert, D. Nowak, A. Isaeva, and T. Doert, Phys. Rev. Mater. **1**, 052001 (2017).
[18] L. Wang, M. Rocci-Lane, P. Brazis, C. R. Kannewurf, Y.-I. Kim, W. Lee, J.-H. Choy, and M. G. Kanatzidis, J. Am. Chem. Soc. **122**, 6629 (2000).
[19] D. Weber, L. M. Schoop, V. Duppel, J. M. Lippmann, J. Nuss, and B. V. Lotsch, Nano Lett. **16**, 3578 (2016).
[20] T. Hyart, A. R. Wright, G. Khaliullin, and B. Rosenow, Phys. Rev. B **85**, 140510(R) (2012).
[21] Y.-Z. You, I. Kimchi, and A. Vishwanath, Phys. Rev. B **86**, 085145 (2012).
[22] J.-W. Mei, Phys. Rev. Lett. **108**, 227207 (2012).
[23] S. Okamoto, Phys. Rev. Lett. **110**, 066403 (2013).
[24] S. Okamoto, Phys. Rev. B **87**, 064508 (2013).
[25] F. Trousselet, P. Horsch, A. M. Oleś, and W.-L. You, Phys. Rev. B **90**, 024404 (2014).
[26] L. Kimme, T. Hyart, and B. Rosenow, Phys. Rev. B **91**, 220501(R) (2015).
[27] J. Schmidt, D. D. Scherer, and A. M. Black-Schaffer, Phys. Rev. B **97**, 014504 (2018).
[28] Y. Hasegawa, T. Aoyama, K. Sasaki, Y. Ikemoto, T. Moriwaki, T. Shirakura, R. Saito, Y. Imai, and K. Ohgushi, J. Phys. Soc. Jpn. **86**, 123709 (2017).
[29] T. Aoyama, Y. Hasegawa, S. Kimura, T. Kimura, and K. Ohgushi, Phys. Rev. B **95**, 245104 (2017).
[30] A. Lerf and R. Schöllhorn, Inorg. Chem. **16**, 2950 (1977).
[31] A. Lerf, F. Sernetz, W. Biberacher, and R. Schöllhorn, Mater. Res. Bull. **14**, 797 (1979).
[32] B. Zhou, Y. Wang, G. B. Osterhoudt, P. Lampen-Kelley, D. Mandrus, R. He, K. S. Burch, and E. A. Henriksen, J. Phys. Chem. Solids **128**, 291 (2019).
[33] K. Takada, H. Sakurai, E. Takayama-Muromachi, F. Izumi, R. A. Dilanian, and T. Sasaki, Nature (London) **422**, 53 (2003).
[34] K. Takada, H. Sakurai, E. Takayama-Muromachi, F. Izumi, R. A. Dilanian, and T. Sasaki, J. Solid State Chem. **177**, 372 (2004).
[35] S. Y. Leung, M. S. Dresselhaus, C. Underhill, T. Krapchev, G. Dresselhaus, and B. J. Wuensch, Phys. Rev. B **24**, 3505 (1981).
[36] K. Momma and F. Izumi, J. Appl. Crystallogr. **44**, 1272 (2011).
[37] J. A. Sears, M. Songvilay, K. W. Plumb, J. P. Clancy, Y. Qiu, Y. Zhao, D. Parshall, and Y.-J. Kim, Phys. Rev. B **91**, 144420 (2015).